Human single-neuron activity is modulated by intracranial theta burst stimulation of the basolateral amygdala

Justin M. Campbell[1,11,*], Rhiannon L. Cowan[2], Krista L. Wahlstrom[3], Martina K. Hollearn[3], Dylan Jensen[1], Tyler Davis[2], Shervin Rahimpour[2], Ben Shofty[2], Amir Arain[4], John D. Rolston[5], Stephan Hamann[6], Shuo Wang[7], Lawrence N. Eisenman[8], James Swift[9,10], Tao Xie[9,10], Peter Brunner[9,10], Joseph R. Manns[6], Cory S. Inman[1,3,12,*], Elliot H. Smith[2,12,*], Jon T. Willie[9,10,12,*]

[1] Interdepartmental Program in Neuroscience, University of Utah, Salt Lake City, UT, USA

[2] Department of Neurosurgery, University of Utah, Salt Lake City, UT, USA

[3] Department of Psychology, University of Utah, Salt Lake City, UT, USA

[4] Department of Neurology, University of Utah, Salt Lake City, UT, USA

[5] Department of Neurosurgery, Brigham and Women's Hospital, Boston, MA, USA

[6] Department of Psychology, Emory University, Atlanta, GA, USA

[7] Department of Radiology, Washington University School of Medicine, St. Louis, MO, USA

[8] Department of Neurology, Washington University School of Medicine, St. Louis, MO, USA

[9] Department of Neurological Surgery, Washington University School of Medicine, St. Louis, MO, USA

[10] National Center for Adaptive Neurotechnologies, St. Louis, MO, USA

[11] Lead contact

[12] Senior author

[*] Corresponding author

Correspondence:

Justin M. Campbell (justin.campbell@hsc.utah.edu)

Cory Inman (cory.inman@psych.utah.edu)

Elliot Smith (e.h.smith@utah.edu)

Jon T. Willie (jontwillie@wustl.edu)

SUMMARY

The amygdala is a highly connected cluster of nuclei with input from multiple sensory modalities, particularly the ventral visual stream, and vast projections to distributed cortical and subcortical regions involved in autonomic regulation and cognition.[1–4] Numerous studies have described the amygdala's capacity to facilitate the encoding of long-lasting emotional memories.[5–15] Recently, direct electrical stimulation of the basolateral complex of the amygdala (BLA) in humans revealed a more generalized ability to enhance declarative memory irrespective of the emotional valence[16], likely by promoting synaptic plasticity-related processes underlying memory consolidation in the hippocampus and medial temporal lobe.[17–20] These effects were achieved with rhythmic theta-burst stimulation (TBS), which is known to induce long-term potentiation (LTP), a key mechanism in memory formation.[21] Emerging evidence suggests that intracranial TBS may also enhance memory specificity[22], evoke theta-frequency oscillations[23], and facilitate short-term plasticity in local field potential recordings.[24,25] However, how amygdalar TBS modulates activity at the single-cell level and to what extent this modulation is associated with memory performance remain poorly understood. Here, we address this knowledge gap by conducting simultaneous microelectrode recordings from prefrontal and medial temporal structures during a memory task in which intracranial TBS was applied to the BLA. We observed a subset of neurons whose firing rate was modulated by TBS and exhibited highly heterogeneous responses with respect to onset latency, duration, and direction of effect. Notably, location and baseline activity predicted which neurons were most susceptible to modulation. These findings provide direct empirical support for stimulation-evoked modulation of single-neuron activity in humans, which has implications for the development and refinement of neuromodulatory therapies.

RESULTS

We recorded single-unit activity from 23 patients (n = 30 sessions) with medically refractory epilepsy as they completed a visual recognition memory task. During the encoding session of the experiment, each patient received either 80 or 160 trials of bipolar intracranial theta burst stimulation (TBS) to a contiguous pair of macroelectrode contacts in the basolateral amygdala (BLA). An equal number of "no-stimulation" trials were randomly interspersed to evaluate the effect of stimulation on memory performance and control for neuronal modulation resulting from experimental stimuli (e.g., image presentation). In total, we isolated 203 putative neurons from 68 bundles of 8 microwires each, distributed among recording sites in the hippocampus (HIP, n = 95 units), orbitofrontal cortex (OFC, n = 44), amygdala (AMY, n = 39), and anterior cingulate cortex (ACC, n = 25); a subset of these units (n = 47, 23.2%) was excluded from subsequent analyses because low baseline firing rates (< 0.1 Hz) limited the ability to robustly detect modulation (*STAR Methods*, *Figure 1;* see also *Figures S1* and *S2* for characterization of detected units).

Theta Burst Stimulation of the BLA Modulates Widely Distributed Populations of Neurons

We hypothesized that BLA stimulation would modulate neuronal activity in the sampled regions, given the amygdala's well-established connectivity to the HIP, OFC, and ACC.[2] To test this hypothesis, we quantified spike counts across trials within peri-stimulation epochs (1 s pre-trial interstimulus interval (ISI), 1 s after image onset, 1 s during stimulation/after image offset, and 1 s post-stimulation) and used Wilcoxon signed-rank tests to compare the spike counts against a null distribution generated by shuffling epoch labels. We performed two firing rate contrasts across trials (pre-trial ISI vs. during stimulation, pre-trial ISI vs. post-stimulation) within two distinct conditions (stim, no-stim); an additional contrast of the pre-trial ISI vs. image onset epochs was included to evaluate the sensitivity of neurons to task image presentations (*STAR Methods*, *Figure 2A*).

BLA TBS modulated firing rates in 30.1% of all recorded units, a significantly higher proportion than the 15.4% responsive to no-stim (image only) trials (one-sided Fisher's

exact test, OR = 2.37, $p < 0.001$; *Figure 3A*). Across all regions sampled, we observed units modulated by the stim and no-stim conditions. Units in HIP (OR = 2.07, $p = 0.044$), OFC (OR = 5.09, $p = 0.040$), and AMY (OR = 3.33, $p = 0.042$) were most sensitive to stimulation; we did not observe a difference in the proportions of units within the ACC responsive to the stim vs. no-stim conditions (OR = 1.00, $p = 0.661$; *Figure 3B*). Only 9.0% of units responded to both the stim and no-stim conditions, despite approximately half of the stim-modulated units (representing 14.7% of all units) exhibiting a change in firing rate associated with image onset (*Figure 3D*). This result suggests that the units modulated by stimulation are largely distinct from those responsive to image offset during trials in which no stimulation was delivered.

Because neuronal firing properties vary across cell types[26–29], we also tested whether baseline (pre-trial ISI) firing rates predicted a unit's response to stimulation, suggestive of selective engagement of specific neuron populations. Stimulation-modulated units exhibited significantly higher baseline firing rates compared to unaffected units ($U(N_{Stim, Mod} = 47, N_{Stim, NS} = 109) = 3450.50$, $p < 0.001$). No difference in baseline firing rate was observed among units modulated in the no-stim condition, compared to those that were unaffected ($U(N_{No\text{-}Stim, Mod} = 24, N_{No\text{-}Stim, NS} = 132) = 1964.00$, $p = 0.062$) (*Figure 3C*). The median (Q1, Q3) baseline firing rates for modulated units in the stim and no-stim conditions were 1.77 Hz (0.95 Hz, 5.39 Hz) and 1.53 Hz (0.72 Hz, 5.41 Hz), respectively.

In a subset of experimental sessions (n = 7), we explored the effects of different stimulation parameters on neuronal modulation within an experimental session (*STAR Methods*); more specifically, we employed a lower stimulation amplitude (0.5 mA vs. 1.0 mA) and varied pulse frequency (33 Hz vs. 50 Hz and 33 Hz vs. 80 Hz). Neither the amplitude of stimulation (OR = 1.69, $p = 0.302$, n = 30) nor pulse frequency (33 vs. 80 Hz; OR = 0.00, $p = 1.000$, n = 1; 50 vs. 80 Hz; OR = 1.40, $p = 0.758$, n = 6) significantly altered the proportion of modulated units. (*Figure S3B*).

Finally, we performed two supplementary analyses to evaluate the robustness of our approach to detecting firing rate modulation: a sensitivity analysis evaluating the proportion of modulated units at different firing rate thresholds for inclusion/exclusion and a data dropout analysis designed to control for the possibility that non-physiological stimulation artifacts may preclude the detection of temporally adjacent spiking (*STAR Methods*). These results recapitulate our observation that units with higher baseline firing are most likely to exhibit modulation and suggest that suppression in firing rate is not solely attributable to amplifier saturation following stimulation (*Figure S4*).

Neurons Exhibit Heterogenous Responses to Theta Burst Stimulation

Recent studies have reported enhanced neural plasticity (via intracranial local field potential recordings and evoked responses) following repetitive direct electrical stimulation.[24,25,30,31] Accordingly, we hypothesized that recorded units would predominantly exhibit enhanced spiking in response to intracranial TBS of the BLA. Unexpectedly, individual units exhibited highly variable responses to stimulation with respect to onset latency (rapid vs. delayed), duration (transient vs. durable), and valence (enhancement vs. suppression) (*Figure 2B*).

The most common epoch for firing rate modulation was during the 1 s epoch in which TBS was delivered (25.0% of all neurons). Smaller subsets were modulated only in the 1 s post-stimulation epoch (6.4%) or in both the during- and post-stimulation epochs (1.3%). A similar trend was observed for modulation in the no-stim condition: 10.9% during, 5.8% post, and 1.3% for both. Suppression was most common among modulated units during stimulation (56.4%), whereas enhancement was the dominant response post-stimulation (70.0%). In contrast, enhancement was most common within both epochs across no-stim trials (58.5% during, 66.7% post). The mean (± SD) absolute z-scored difference in firing rate across stimulation trials (relative to pre-trial ISI) was z=0.60 (± 0.58) and z=0.43 (± 0.27) for the during- and post-stimulation epochs, respectively. Across no-stim trials, we observed a mean absolute z-scored difference of z=0.38 (± 0.24) and z=0.30 (± 0.18) in analogous epochs (*Figure 3E*).

Association Between Neuronal Modulation and Memory Performance is Unclear

Next, we performed an exploratory analysis to investigate the link between stimulation-evoked neuronal modulation and subsequent performance during the visual recognition memory task. To this end, we first used a linear mixed-effects model to examine the effect of condition (stim, no-stim) on memory performance (d') across trials in each session, with individual sessions treated as a random effect (i.e., intercept). Experiment type was also included as a fixed effect since data were aggregated across four highly similar experiments with minor differences in the content of visual stimuli, number of trials, stimulation parameters, and testing intervals (*STAR Methods*). However, we did not observe an overall effect of memory enhancement ($p > 0.05$) when controlling for subject-level variability (*Figure 4A*). The lack of a memory enhancement effect could be attributed to high hit rates (mean ± SD) (75.7% ± 13.5% for no-stim trials, 75.0% ± 14.3% for stim trials), and considerable variability among false alarm rates (17.9% ± 17.4%, range 0–70%; *Figure 4B*) across participants.

To test our hypothesis that modulation of neurons would be associated with changes in memory performance, we combined the sessions that resulted in either memory enhancement or impairment and contrasted the proportion of modulated units across regions sampled; a threshold of Δd' ± 0.2 was chosen based on the defined range of a "small effect" for Cohen's *d*. At the level of individual sessions, we observed enhanced memory (Δd' > +0.2) in 43.3%, impaired memory (Δd' < -0.2) in 36.7%, and negligible change (-0.2 ≤ Δd' ≤ 0.2) in 20.0% when comparing performance between the stimulation and image-only conditions**.** We did not, however, observe a meaningful difference in the proportion of modulated units when grouped by behavioral outcome (all $p > 0.05$) (*Figure 4C*).

DISCUSSION

Theta-burst stimulation is an efficient and validated paradigm for inducing long-term potentiation (LTP) in neural circuits.[21] Additionally, intracranial TBS was recently shown

to promote region-specific short-term plasticity[24,25] and entrain frequency-matched oscillations.[23] At present, however, there is an incomplete understanding of how these population-level responses to stimulation relate to a modulation in the activity of individual neurons, which are thought to be the substrate of memory encoding and retrieval.[32] Here, we address this knowledge gap by characterizing neuronal firing recorded from microelectrodes in humans undergoing intracranial TBS of the amygdala. Our experimental design focused specifically on stimulation of the BLA, given our prior work that seeks to understand amygdala-mediated memory enhancement in humans.[16,33,34]

We observed neurons distributed throughout the hippocampus, orbitofrontal cortex, anterior cingulate cortex, and amygdala that were responsive to direct electrical TBS. The effect of TBS on firing rate was heterogeneous with respect to onset, duration, and valence. Previous work characterizing local-field potential responses to intracranial TBS observed similarly bidirectional effects throughout the brain suggestive of short-term plasticity.[25] Few studies, however, have characterized the effects of exogenous stimulation on the spiking activity of individual neurons. One study reported a long-lasting reduction in neural excitability among parietal neurons, with variable onset time and recovery following continuous transcranial TBS in non-human primates.[35] Other emerging evidence suggests that transcranial direct current stimulation may entrain neuronal spiking[36] and that stimulation-evoked modulation of spiking may meaningfully impact behavioral performance on cognitive tasks.[37] An alternative approach has focused on the delivery of spatially selective microstimulation resembling the extracellular currents that normally modulate neuronal activity—this methodology has been used to bidirectionally drive neuronal firing in human temporal cortex[38] and enhance memory specificity for images following stimulation.[22]

Although subsets of neurons from each region we sampled were responsive to stimulation, we observed the greatest difference in the proportion of modulated units across conditions in the hippocampus, orbitofrontal cortex, and amygdala. This regional selectivity is to be expected, given that numerous studies have characterized how

structural, functional, and effective connectivity among brain regions predicts the effects of stimulation.[25,30,31,39–42] We also observed that units with greater baseline activity were most likely to exhibit modulated firing rates following stimulation. Other studies have identified firing patterns and waveform properties that differ between inhibitory and excitatory neurons in humans.[26–29] For example, baseline firing rate disambiguates "regular-spiking" and "fast-spiking" neurons, which are presumed to represent pyramidal cells and interneurons, respectively. This may suggest that inhibitory interneurons are especially sensitive to TBS. However, further analysis of waveform properties (e.g., valley-to-peak height, half-peak width) is needed to more reliably classify neuronal cell types. Future research that seeks to identify specific characteristics of human neurons that predict responses to stimulation would be informative, given recent reports that the extent to which electrical fields entrain neuronal spiking may be specific to distinct classes of cells.[43]

Modulation in neuronal activity was defined by contrasting firing rates before, during, and after TBS across trials. In doing so, we were able to characterize coarse differences in activity indicative of enhancement or suppression. This approach, however, did not allow for analysis of more subtle, nuanced effects such as entrainment of spiking to individual bursts or pulses of TBS. Characterizations of rhythmicity in firing were challenging in this experiment, given that most of the neurons we identified exhibit sparse activity with low baseline firing rates, and stimulation often resulted in further suppression of spiking.

Although stimulation artifacts generally resulted in amplitude threshold crossings that may be spuriously interpreted as a neuronal spike, we implemented several methods to mitigate the influence of non-physiological activity. First, the characteristics of each unit (e.g., waveform shape) were manually inspected during spike sorting and further quantified using several quality control metrics (e.g., interspike intervals); stimulation resulted in a stereotyped response that was easily detectable and removed from subsequent analyses. Additionally, we tested for modulation during stimulation but also within the post-stimulation epochs—a period in which no artifact was present. Contrary to

what would be expected if stimulation artifact was the explanation for firing rate changes, we observed predominantly suppression during stimulation and enhancement post-stimulation.

Recent studies have characterized specific oscillatory dynamics in the amygdalohippocampal circuit responsible for prioritizing the encoding of salient memories.[14,15,44] Since we collected our microelectrode recordings in the context of a visual recognition memory task, we tested for associations between neuronal modulation and the change in memory performance attributable to TBS. We hypothesized that robust modulation in firing rate would be predictive of a stimulation-related memory effect, whether impairment or enhancement. However, we did not observe a clear link between modulation and behavioral outcome. The absence of such an effect may be related to limitations with sparse recordings[45], or at least in part, attributable to the considerable variability among the change in memory performance from stimulation that we observed in this dataset. Indeed, we did not identify an apparent stimulation-related memory enhancement when controlling for individual differences, in contrast to our prior work.[16]

Several studies on rats have demonstrated that brief electrical stimulation of the BLA can prioritize the consolidation of specific memories.[46–49] These pro-memory effects emerged ~24 hours post-encoding and appear to be hippocampal-dependent[47], despite not resulting in a net change in the firing rates of hippocampal pyramidal neurons; instead, BLA stimulation resulted in brief periods of spike-field and field-field synchrony within CA3–CA1 in the low-gamma frequency range (30–55 Hz), which may facilitate spike-timing-dependent plasticity in recently active neurons.[48]

The present study did not investigate interactions between spiking activity and local field potentials. How exactly the activity of single neurons is aggregated to produce local field potentials, which in turn interact with neuronal ensembles distributed throughout the brain, remains an active area of research.[50–53] One recent study that leveraged closed-loop stimulation targeting memory consolidation during sleep observed neuronal spiking with

greater phase-locking to medial temporal lobe slow-wave activity following stimulation[54]; neuronal phase-locking, particularly to hippocampal theta oscillations, has long been associated with robust memory encoding and retrieval.[55–58] Further characterization of these spike-field interactions and refinement of closed-loop stimulation methods may provide a means for precisely modulating neuronal dynamics, for example, by entraining neuronal spiking that is phase-aligned to endogenous hippocampal theta oscillations to selectively enhance the encoding or retrieval of memories.[59–62] This level of precision could, in turn, facilitate more consistent memory effects with intracranial stimulation.

Conclusions

By characterizing patterns of neuronal modulation evoked by intracranial TBS, we provide new insights that link micro- and macroscale responses to stimulation of the human brain. These insights advance our limited understanding of how focal electrical fields influence neuronal firing at the single-cell level and motivate future neuromodulatory therapies that aim to recapitulate specific patterns of activity implicated in cognition and memory.

STAR METHODS

KEY RESOURCES TABLE

REAGENT or RESOURCE	SOURCE	IDENTIFIER
Software and algorithms		
Custom Python code	This paper	https://github.com/Justin-Campbell/BLAESUnits
Scipy	[63]	https://scipy.org
Statsmodels	[64]	https://statsmodels.org
Seaborn	[65]	https://seaborn.pydata.org
Offline Sorter	Plexon Inc	https://plexon.com/products/offline-sorter/
LeGUI	[66]	https://github.com/Rolston-Lab/LeGUI
BCI2000	National Center for Adaptive Neurotechnologies	https://bci2000.org
Other		
Data acquisition system	Blackrock Neurotech	NeuroPort™
Data acquisition system	Nihon Koden	EEG-1260 Amplifier
Neurostimulator	Blackrock Neurotech	Cerestim
Stereo-EEG electrodes	Ad-Tech Medical	Macro-Micro Depth Electrodes

RESOURCE AVAILABILITY

Lead Contact

Further information and requests for resources should be directed to the lead author, Justin M. Campbell (justin.campbell@hsc.utah.edu).

Data and Code Availability

Custom Python analysis scripts used in the manuscript are publicly available on GitHub (https://github.com/Justin-Campbell/BLAESUnits). Deidentified neural recordings may be made available upon reasonable request.

Materials Availability

This study did not generate new materials or reagents.

EXPERIMENTAL MODEL AND SUBJECT DETAILS

We report results from a cohort of 23 patients with medically refractory epilepsy who underwent stereoelectroencephalography to localize epileptogenic foci (74% female, 19–66 years old). All patients were age 18+ and able to provide informed consent. No exclusion was made concerning a patient's sex, gender, race, ethnicity, or socioeconomic status.

Surgeries were performed at the University of Utah in Salt Lake City, UT (n = 10) and Barnes-Jewish Hospital in St. Louis, MO (n = 13). Patients were monitored continuously by a clinical team during their post-operative hospital course. Each patient signed a written informed consent form before participation in the research study; all study procedures were approved by the Institutional Review Board at the University of Utah (IRB 00144045, IRB 00114691) and Washington University (IRB 202104033).

METHOD DETAILS

Electrode Placement and Localization

Numbers and trajectories of stereoelectroencephalography electrode placements were determined case-by-case and solely derived from clinical considerations during a multidisciplinary case conference without reference to this research program. Each patient was implanted with clinical macroelectrodes and 1–3 Behnke-Fried depth electrodes (Ad-Tech Medical Instrument Corporation, Oak Creek, WI), which contained both macro- and microelectrode contacts (eight 40 μm diameter microwires and one unshielded reference wire) for recording local field potentials and extracellular action potentials, respectively (Figure 1A). To localize electrodes, we leveraged the open-access *Localize Electrodes Graphical User Interface (LeGUI)*[66] software developed by our group, which performs coregistration of pre-operative MRI and post-operative CT sequences, image processing, normalization to standard anatomical templates, and automated electrode detection.

Intracranial Electrophysiology

At both hospitals, neurophysiological data were recorded using a neural signal processor (Blackrock Microsystems, Salt Lake City, UT; Nihon Koden USA, Irvine, CA) sampling at 30 kHz. Microelectrode contacts were locally referenced to a low-impedance microwire near the recording wires. Macroelectrode contacts were referenced to an intracranial contact located within the white matter with minimal activity, per recommended practices.[67]

Experimental Design

Patients completed a visual recognition memory task previously employed by our group to characterize the effects of basolateral amygdala stimulation upon memory consolidation.[16] The memory task consisted of an encoding session, during which a series of neutral valence images were presented, and a self-paced retrieval session ~24 hours post-encoding wherein patients were asked to indicate whether each image onscreen was old (previously shown) or new (unseen) (*Figure 2A*). Data were aggregated across four highly similar experimental paradigms with minor differences in the content of visual stimuli, number of trials, stimulation parameters, and testing intervals. Each encoding session consisted of either 160 or 320 trials wherein an image was presented on screen for 3 s, followed by a jittered interstimulus interval of 6.5–7.5 s (fixation cross on screen). A random half of the encoding trials were immediately followed by 1 s of basolateral amygdala stimulation (described in *Intracranial Theta Burst Stimulation*).

Intracranial Theta Burst Stimulation

We delivered direct electrical stimulation to the basolateral amygdala during half of the trials in the encoding phase of each experimental session. Stimulation pulses were delivered immediately once the image was removed from the screen and in a patterned rhythm designed to entrain endogenous theta-gamma oscillatory interactions (theta-burst stimulation, TBS).[68,69] Specifically, we administered charge-balanced, bipolar, 1 mA, biphasic rectangular pulses over a 1 s period with a 50% duty cycle. Stimulation pulses were delivered at a rate of 50 Hz and nested within eight equally-spaced bursts (~ 8 Hz)

(*Figure 2B-C*). A subset of experiments (n = 7) used a lower current (0.5 mA) with variable pulse frequencies across trials (33 Hz, 50 Hz, 80 Hz).

Spike Detection and Sorting

Microelectrode data were first filtered between 250–500 Hz with a zero-phase lag bandpass filter and re-thresholded offline at -3.5 times the root mean square of the signal to identify spike waveforms. Units were isolated during a semi-automated process within *Offline Sorter* (Plexon Inc, Dallas, TX) by applying the T-distribution expectation maximization method on the first three principal components of the detected waveforms (initial parameters: degrees of freedom multiplier = 4, initial number of units = 3).[70] Finally, the waveform shapes, interspike interval distribution, consistency of firing, and isolation from other waveform clusters were manually inspected for further curation and removal of spurious, non-physiological threshold crossings that could represent stimulation artifact.

QUANTIFICATION AND STATISTICAL ANALYSIS

Single Unit Quality Metrics

We calculated several distinct metrics to characterize detected units' properties and assess the quality of our spike sorting (*Figure S1*). A: the number of units detected per microelectrode bundle, B: the mean firing rate (Hz) for each unit, C: the percentage of interspike intervals < 3 ms, D: the coefficient of variation across each unit's spike train, E: the average presence ratio of firing in 1s bins (proportion of bins which contain ≥ 1 spike), F: the ratio between the peak amplitude of the averaged waveform and its standard deviation, G: the mean signal-to-noise ratio of the averaged waveform.

Peri-Stimulation Firing Rate Analyses

We first created peri-stimulation epochs (1 s pre-trial ISI, 1 s after image onset, 1 s during stimulation/after image offset, 1 s post-stimulation), with t = 0 representing stimulation onset and the moment at which the image was removed from the screen (*Figure 2A*); identical epochs were created for the image-only (no-stimulation) trials. Units with a trial-

averaged baseline (pre-trial ISI) firing rate of < 0.1 Hz were excluded from subsequent analyses because low firing rates limited the ability to robustly detect modulation. Units were designated as "modulated" if either the during- or post-stimulation firing rate contrast was significant following permutation testing (described in *Statistical Analyses*). An additional contrast of pre-trial ISI vs. image onset was performed to evaluate the sensitivity of neurons to task stimuli (i.e., image presentation).

Firing Rate Control Analyses

We performed a sensitivity analysis by systematically varying the baseline firing rate threshold used to exclude units from modulation analyses. The threshold for inclusion of units was varied from 0–3 Hz (0.1 Hz step size), and the firing rate analyses were repeated to quantify the proportion of units meeting inclusion criteria and the proportion of units designated as modulated (*Figure S4A*). Next, we performed a dropout analysis wherein segments of data near the onset of a stimulation burst were removed from the during-stimulation epoch (an identical segment was also removed from the pre-trial ISI and post-stimulation epochs). To this end, we removed a window of data starting at the onset of each burst spanning 0–60 ms (5 ms step size, eight bursts in train) and recomputed the proportion of units meeting inclusion criteria and the proportion of units designated as modulated (*Figure S4B*).

Statistical Approach

All statistical analyses were conducted using custom Python scripts and established statistical libraries (i.e., *scipy*[63]*, statsmodels*[64]). We performed two separate Wilcoxon signed-rank tests (*scipy.stats.wilcoxon*) across trials on the during- and post-stimulation spike counts relative to their corresponding pre-trail baseline spike counts. To control for false positives, we compared the empirical test statistic against a null distribution generated from shuffling pre/during/post epoch labels (n = 1000 permutations) (*Figure 2B*). An identical analysis was also performed on the no-stimulation (image-only) trials.

To test for differences in the proportion of modulated units (across conditions, regions, stimulation parameters, and behavioral outcomes), we performed a series of one- and two-sided Fisher's exact tests (*scipy.stats.fisher_exact*) (*Figure 3A-B, Figure 4C*, *Figure S3*). Next, we used Mann-Whitney U tests to contrast baseline firing rates among modulated vs. unaffected units (*scipy.stats.mannwhitneyu*) (*Figure 3C*). Behavioral performance during the memory task was calculated using d-prime (d'), defined as the difference in an individual's z-scored hit rate and false alarm rate. Observed changes in recognition memory were split into two categories using a d' difference threshold of ± 0.2: responder ($\Delta d' < -.2$ or $\Delta d' > +.2$) or non-responder ($-0.2 \leq \Delta d' \leq 0.2$). The threshold of ± 0.2 was chosen based on the defined range of a "small effect" for Cohen's *d,* which bears conceptual similarity to d'. To test the hypothesis that stimulation affected behavioral performance, we used a linear mixed effects model with d' score as the dependent variable, condition and experiment as fixed effects, and session as a random effect (*statsmodels.regression.mixed_linear_model.MixedLM*) (*Figure 4A*); an additional test for differences among hit rates (percent of previously seen images correctly identified) was implemented using a paired-samples t-test (*scipy.stats.ttest_rel*) (*Figure 4B*).

Highlights

- Individual neurons in the human brain were responsive to theta burst stimulation
- Basolateral amygdala stimulation preferentially modulated neurons in the hippocampus, orbitofrontal cortex, and amygdala
- Neurons modulated by stimulation tended to have greater baseline firing rates
- Duration, onset, and valence of neuronal modulation were heterogeneous

In Brief

Campbell et al. identify a subset of neurons in humans whose firing rate is modulated by intracranial theta burst stimulation of the basolateral amygdala. Location and baseline activity of detected neurons were associated with responsiveness to stimulation. These results provide a link between micro- and macroscale responses evoked by stimulation.

Keywords

- Intracranial EEG
- Single-unit
- Theta burst stimulation
- Modulation
- Amygdala

Acknowledgments

This work was supported by the National Institute of Neurological Disorders and Stroke (T32NS115723; K23NS114178), the National Institute of Mental Health (R01MH120194), the National Science Foundation (NSF2124252, NSF1747505), and the Brain & Behavior Research Foundation (2023 NARSAD Young Investigator Grant). We are also deeply grateful to the patients who participated in this research program.

CRediT Author Statement

Justin Campbell: Conceptualization, Methodology, Software, Formal Analysis, Investigation, Data Curation, Writing – Original Draft, Writing – Review & Editing,

Visualization; **Rhiannon Cowan**: Conceptualization, Data Curation, Writing – Review & Editing; **Krista Wahlstrom**: Investigation, Writing – Review & Editing, Project Administration; **Martina Hollearn**: Writing – Review & Editing; **Dylan Jensen**: Writing – Review & Editing; **Tyler Davis**: Software, Writing – Review & Editing; **Shervin Rahimpour**: Resources, Writing – Review & Editing; **Ben Shofty**: Resources, Writing – Review & Editing; **Amir Arain**: Resources, Writing – Review & Editing; **John Rolston**: Resources, Writing – Review & Editing; **Stephan Hamann**: Writing – Review & Editing; **Shuo Wang**: Resources, Writing – Review & Editing; **Lawrence Eisenman**: Resources, Writing – Review & Editing; **James Swift**: Software, Investigation, Writing – Review & Editing; **Tao Xie**: Investigation, Writing – Review & Editing; **Peter Brunner**: Software, Investigation, Supervision, Writing – Review & Editing; **Joe Manns**: Conceptualization, Supervision, Project Administration, Writing – Review & Editing; **Cory Inman**: Supervision, Resources, Project Administration, Funding Acquisition, Writing – Review & Editing; **Elliot Smith**: Conceptualization, Supervision, Resources, Writing – Review & Editing; **Jon Willie**: Investigation, Supervision, Resources, Project Administration, Funding Acquisition, Writing – Review & Editing.

Competing Interests

None.

Supplemental Information

Supplemental Figures 1–4.

Additional Resources

This study was conducted as part of a National Institutes of Health clinical trial (NCT05065450).

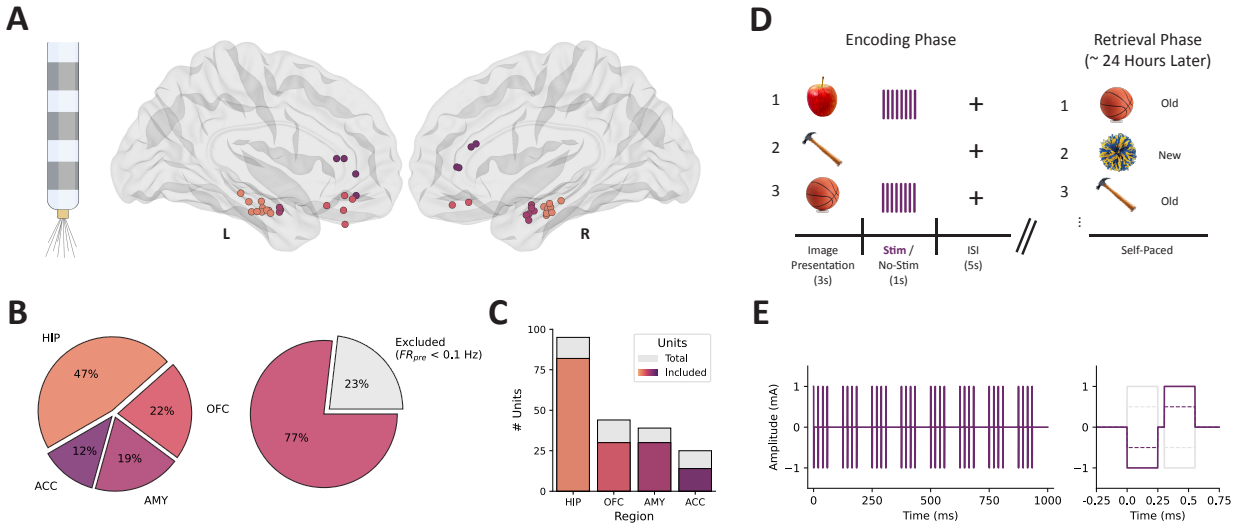

Figure 1: Microelectrode locations, unit counts, and experimental design.

(A) Behnke Fried-style macro/micro depth electrode (left) and microelectrode bundle locations projected in MNI space (right). (B) The proportion of units recorded from each brain area (left) and the proportion of units that met the criteria for inclusion in analyses (average pre-trial baseline firing rate ≥ 0.1 Hz) (right). (C) Counts of total (grey) and included (colored) units within each region. (D) Intracranial recording and stimulation took place in the context of a two-phase (encoding, retrieval) visual recognition memory task. A series of neutral valence images were shown (3 s), half of which were followed by direct electrical stimulation (1 s). Retrieval memory was tested during a self-paced task ~24 hours later. (E) Simulated theta-burst stimulation trace (left) and individual stimulation pulse (right); charge-balanced, bipolar, biphasic rectangular pulses were delivered over a 1 s period.

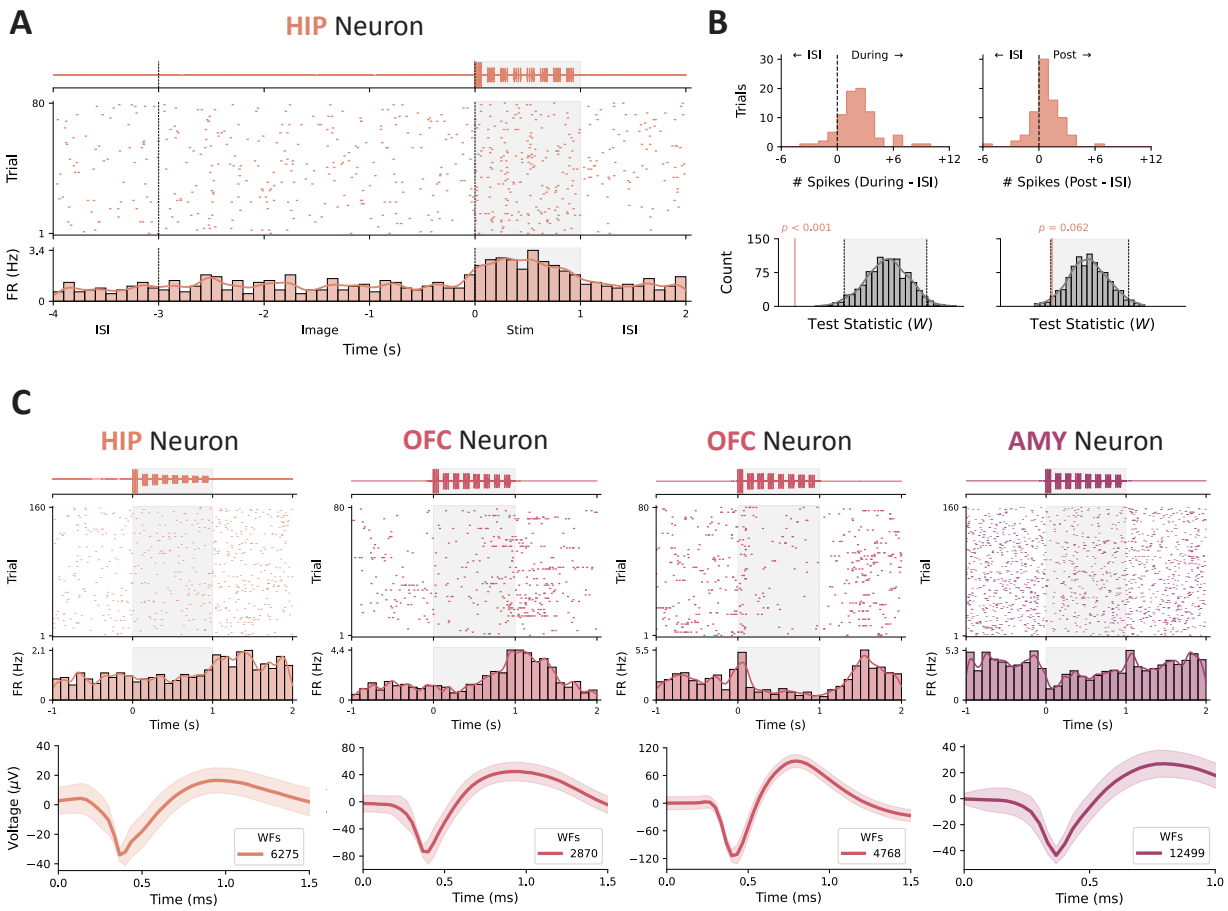

Figure 2: Example raster plots depicting heterogeneous responses to stimulation. (A) Representative example of modulation during stimulation. The highpass-filtered, trial-averaged LFP from the corresponding microwire is shown (top) above the spike raster for an example unit located in the hippocampus (middle); the grey shaded region depicts the duration of stimulation with onset at t = 0. The average firing rate across trials was estimated by convolving the binned spike counts (100 ms bins) with a Gaussian kernel (bottom). (B) The difference in the number of spikes in the 1 s peri-stimulation epochs for each trial is shown (top). We subsequently performed a Wilcoxon signed-rank test on the during- and post-stimulation spike counts for each trial vs. the pre-trial baseline and compared the empirical test statistic against a null distribution generated by shuffling the epoch labels 1,000 times (bottom); the grey-shaded region represents the distribution containing 95% of observed values. (C) Some units (left, left-middle) exhibited increased

firing rates, whereas others (right-middle, right) had their firing suppressed. The temporal dynamics of the firing rate modulation (e.g., onset, duration) were highly variable across units. The averaged waveform for each of the visualized units is shown below its corresponding peri-stimulation raster plot (WFs = waveforms); the shaded region represents standard deviation across waveforms.

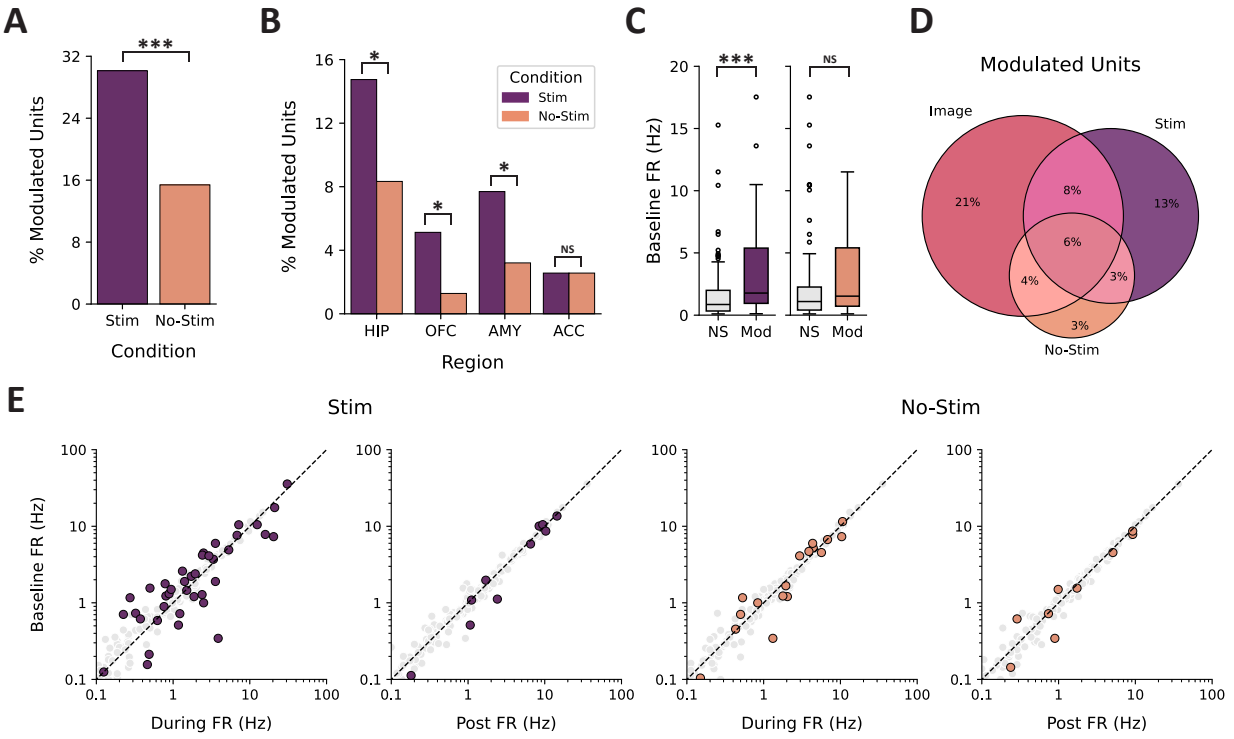

Figure 3: Characterization of modulation in neuronal firing rate.

(A) Percent of modulated units observed across trials separated by stim (purple) vs. no-stim conditions (orange). (B) Percent of modulated units as a function of recording region. (C) Comparison of baseline firing rate in units separated by condition (stim vs. no-stim) and outcome (NS = not significant, Mod = modulated). (D) Venn diagram depicting the shared and independent proportions of units modulated by image onset (Image) and the two experimental conditions (stim vs. no-stim). (E) Scatterplot of pre-stimulation firing rate relative to the firing rate during the two contrast windows (during, post) for the stim (left) and no-stim (right) conditions. Modulated units are highlighted in purple (stim) or orange (no-stim). * $p < 0.05$, *** $p < 0.001$, NS = not significant.

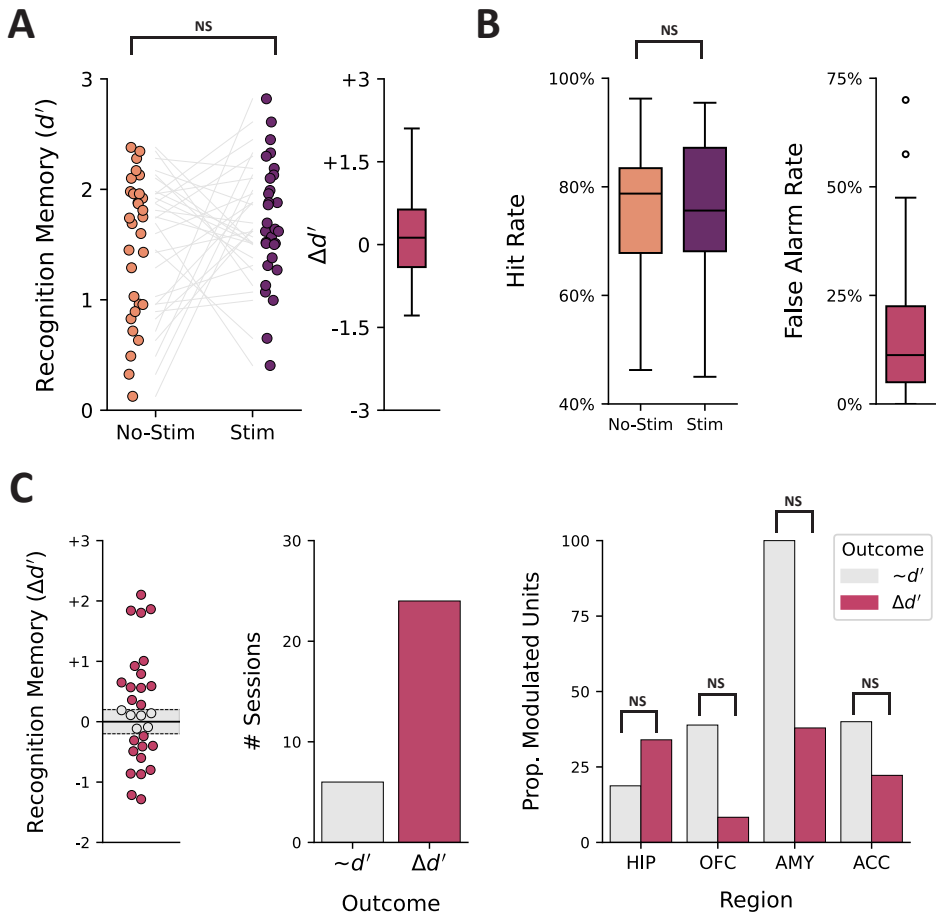

Figure 4: Summary of behavioral performance during memory task.

(A) Memory performance for each session is quantified using d' (left); grey lines connect d' scores across conditions for an individual session. Boxplot of the observed difference in d' scores across conditions (right). (B) Hit rate (percent of old images correctly recognized) and false alarm rate (percent of new images incorrectly labeled as old) across conditions. (C) Change in recognition memory performance was split into two categories using a d' difference threshold of ± 0.2: responder (positive or negative; Δd', pink) and non-responder (~d', grey). Individual d' scores are shown (left) with points colored by outcome category; dotted lines demarcate category boundaries, and the grey-shaded region represents negligible change. The number of sessions within each outcome category (middle) and the proportion of modulated units as a function of outcome category, separated by region (right). NS = not significant.

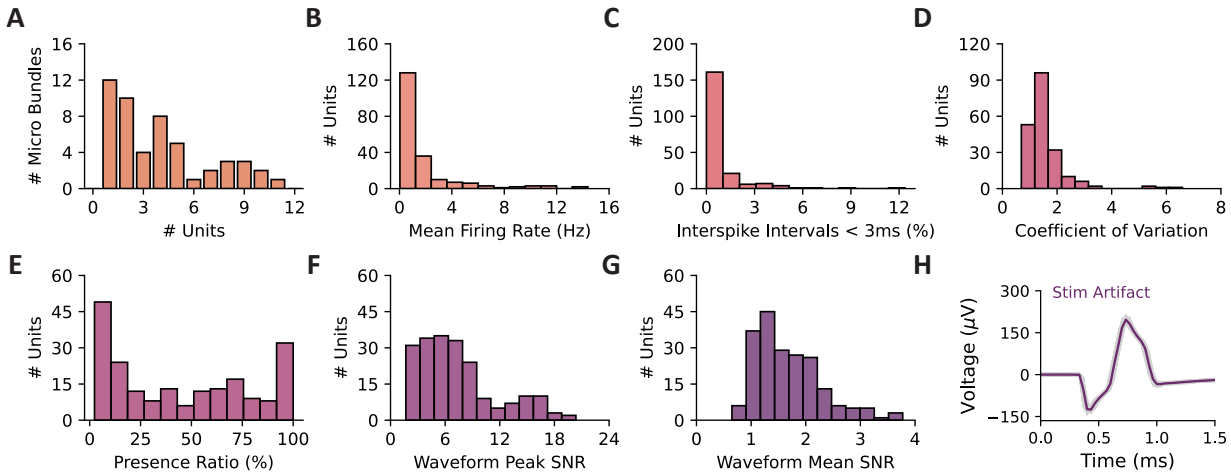

Supplemental Figure 1: Unit quality metrics.

(A) Number of units detected per implanted microelectrode bundle. (B) Mean firing rate (Hz) across recording session. (C) Percent of interspike intervals < 3 ms. (D) Interspike interval coefficient of variation. (E) Mean presence ratio of firing within units (1 s bins). (F) Signal-to-noise ratio of unit waveform peak. (G) Mean signal-to-noise ratio across the entire unit waveform. (H) Representative example of stereotyped, high-amplitude stimulation-artifact waveform; non-physiological waveforms were excluded from analysis.

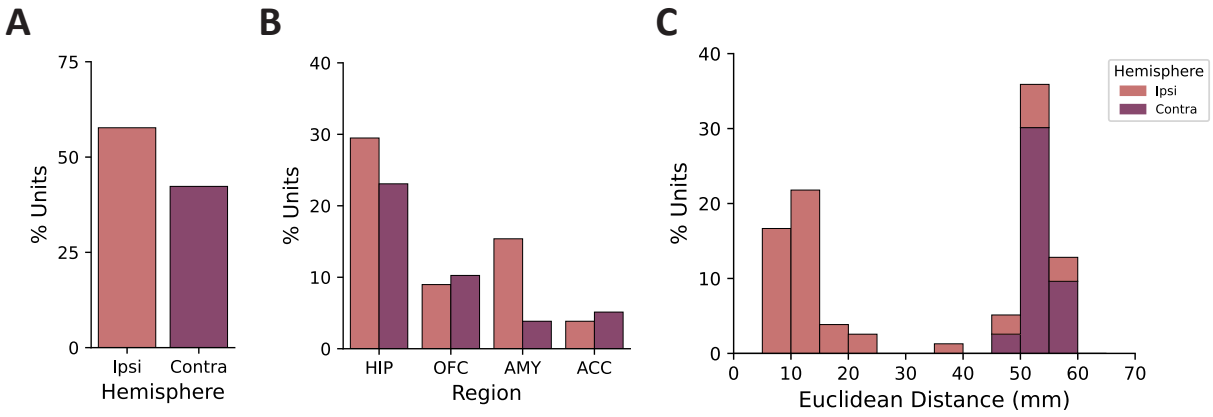

Supplemental Figure 2: Characterization of units based on laterality relative to stimulation.

(A) Unit counts on the contralateral (Contra) or ipsilateral (Ipsi) side of stimulation. (B) Unit counts separated by laterality and region. (C) Stacked histograms of Euclidean distance between microelectrode bundle location and stimulation contacts, separated by laterality (bin size = 5 mm).

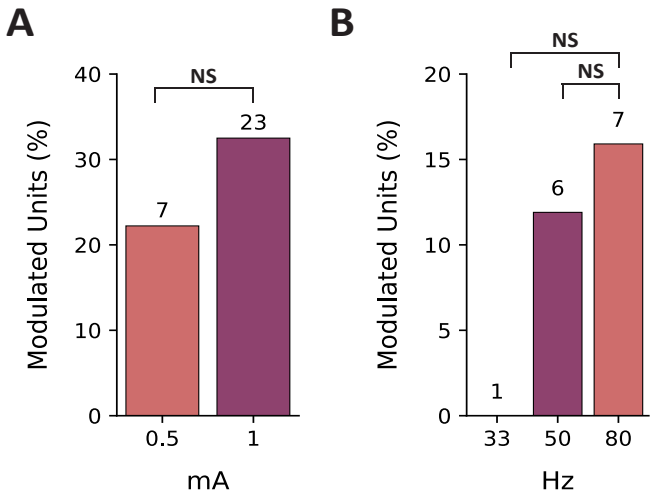

Supplemental Figure 3: Sub-analysis of stimulation parameters used across experiments.

A subset of experiments (n = 7) used a lower amperage of stimulation (0.5 mA vs. 1 mA) and two distinct pulse frequencies across trials: 33 Hz vs. 80 Hz (n = 1) and 50 Hz vs. 80 Hz (n = 6). (A) Comparison of the proportion of stimulation-modulated units across sessions with 1 mA (n = 23) vs. 0.5 mA (n = 7). (B) Comparison of the proportion of stimulation-modulated units across sessions testing distinct pulse frequencies (n = 7). The values above individual bars represent the number of sessions using that stimulation parameter. NS = not significant.

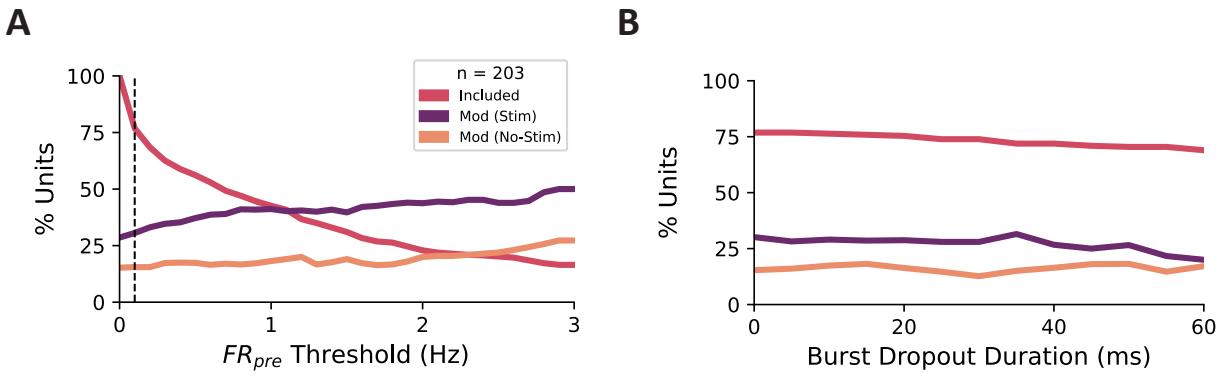

Supplemental Figure 4: Control analyses for the detection of modulated units.

The same permutation-based analyses reported in the manuscript were repeated under different control conditions; the percent of units (total n = 203) that met the ≥ 0.1 Hz firing rate threshold for inclusion (pink), the percent of included units modulated in the stim condition (purple), and the percent of included units modulated in the no-stim condition are shown. (A) The threshold for inclusion of units was varied from 0–3 Hz (0.1 step size); the black dashed line represents the 0.1 Hz threshold used in the manuscript. (B) To control for the possibility that non-physiological stimulation artifacts may preclude the detection of temporally adjacent spiking, we removed segments of data beginning at the onset of each burst of pulses (0–60 ms, 5 ms step size). Identical temporal windows were removed from the corresponding pre- and post-stimulation epochs to mitigate effects resulting solely from summation over different epoch sizes (reduced spike counts with shorter windows).

References

1. Stein, J.L., Wiedholz, L.M., Bassett, D.S., Weinberger, D.R., Zink, C.F., Mattay, V.S., and Meyer-Lindenberg, A. (2007). A validated network of effective amygdala connectivity. NeuroImage *36*, 736–745. https://doi.org/10.1016/j.neuroimage.2007.03.022.

2. Roy, A.K., Shehzad, Z., Margulies, D.S., Kelly, A.M.C., Uddin, L.Q., Gotimer, K., Biswal, B.B., Castellanos, F.X., and Milham, M.P. (2009). Functional connectivity of the human amygdala using resting state fMRI. NeuroImage *45*, 614–626. https://doi.org/10.1016/j.neuroimage.2008.11.030.

3. Kim, M.J., Loucks, R.A., Palmer, A.L., Brown, A.C., Solomon, K.M., Marchante, A.N., and Whalen, P.J. (2011). The structural and functional connectivity of the amygdala: From normal emotion to pathological anxiety. Behav. Brain Res. *223*, 403–410. https://doi.org/10.1016/j.bbr.2011.04.025.

4. McDonald, A.J., and Mott, D.D. (2017). Functional neuroanatomy of amygdalohippocampal interconnections and their role in learning and memory. J. Neurosci. Res. *95*, 797–820. https://doi.org/10.1002/jnr.23709.

5. Phelps, E.A. (2004). Human emotion and memory: interactions of the amygdala and hippocampal complex. Curr. Opin. Neurobiol. *14*, 198–202. https://doi.org/10.1016/j.conb.2004.03.015.

6. Dolcos, F., LaBar, K.S., and Cabeza, R. (2004). Interaction between the Amygdala and the Medial Temporal Lobe Memory System Predicts Better Memory for Emotional Events. Neuron *42*, 855–863. https://doi.org/10.1016/s0896-6273(04)00289-2.

7. Richardson, M.P., Strange, B.A., and Dolan, R.J. (2004). Encoding of emotional memories depends on amygdala and hippocampus and their interactions. Nat. Neurosci. *7*, 278–285. https://doi.org/10.1038/nn1190.

8. Phelps, E.A., and LeDoux, J.E. (2005). Contributions of the Amygdala to Emotion Processing: From Animal Models to Human Behavior. Neuron *48*, 175–187. https://doi.org/10.1016/j.neuron.2005.09.025.

9. Phelps, E.A. (2006). Emotion and Cognition: Insights from Studies of the Human Amygdala. Annu. Rev. Psychol. *57*, 27–53. https://doi.org/10.1146/annurev.psych.56.091103.070234.

10. LaBar, K.S., and Cabeza, R. (2006). Cognitive neuroscience of emotional memory. Nat. Rev. Neurosci. *7*, 54–64. https://doi.org/10.1038/nrn1825.

11. Roozendaal, B., McEwen, B.S., and Chattarji, S. (2009). Stress, memory and the amygdala. Nat. Rev. Neurosci. *10*, 423–433. https://doi.org/10.1038/nrn2651.

12. Schwabe, L., Tegenthoff, M., Höffken, O., and Wolf, O.T. (2013). Mineralocorticoid Receptor Blockade Prevents Stress-Induced Modulation of

Multiple Memory Systems in the Human Brain. Biol. Psychiatry *74*, 801–808. https://doi.org/10.1016/j.biopsych.2013.06.001.

13. Hermans, E.J., Battaglia, F.P., Atsak, P., Voogd, L.D. de, Fernández, G., and Roozendaal, B. (2014). How the amygdala affects emotional memory by altering brain network properties. Neurobiol. Learn. Mem. *112*, 2–16. https://doi.org/10.1016/j.nlm.2014.02.005.

14. Zheng, J., Anderson, K.L., Leal, S.L., Shestyuk, A., Gulsen, G., Mnatsakanyan, L., Vadera, S., Hsu, F.P.K., Yassa, M.A., Knight, R.T., et al. (2017). Amygdala-hippocampal dynamics during salient information processing. Nat Commun *8*, 14413. https://doi.org/10.1038/ncomms14413.

15. Qasim, S.E., Mohan, U.R., Stein, J.M., and Jacobs, J. (2023). Neuronal activity in the human amygdala and hippocampus enhances emotional memory encoding. Nat. Hum. Behav. *7*, 754–764. https://doi.org/10.1038/s41562-022-01502-8.

16. Inman, C.S., Manns, J.R., Bijanki, K.R., Bass, D.I., Hamann, S., Drane, D.L., Fasano, R.E., Kovach, C.K., Gross, R.E., and Willie, J.T. (2018). Direct electrical stimulation of the amygdala enhances declarative memory in humans. Proc National Acad Sci *115*, 98–103. https://doi.org/10.1073/pnas.1714058114.

17. McGaugh, J.L., McIntyre, C.K., and Power, A.E. (2002). Amygdala Modulation of Memory Consolidation: Interaction with Other Brain Systems. Neurobiol Learn Mem *78*, 539–552. https://doi.org/10.1006/nlme.2002.4082.

18. McGaugh, J.L. (2004). The Amygdala Modulates The Consolidation of Memories of Emotionally Arousing Experiences. Annu. Rev. Neurosci. *27*, 1–28. https://doi.org/10.1146/annurev.neuro.27.070203.144157.

19. McGaugh, J.L. (2013). Making lasting memories: Remembering the significant. Proc. Natl. Acad. Sci. *110*, 10402–10407. https://doi.org/10.1073/pnas.1301209110.

20. Roesler, R., Parent, M.B., LaLumiere, R.T., and McIntyre, C.K. (2021). Amygdala-hippocampal interactions in synaptic plasticity and memory formation. Neurobiol. Learn. Mem. *184*, 107490. https://doi.org/10.1016/j.nlm.2021.107490.

21. Larson, J., and Munkácsy, E. (2015). Theta-burst LTP. Brain Res. *1621*, 38–50. https://doi.org/10.1016/j.brainres.2014.10.034.

22. Titiz, A.S., Hill, M.R.H., Mankin, E.A., Aghajan, Z.M., Eliashiv, D., Tchemodanov, N., Maoz, U., Stern, J., Tran, M.E., Schuette, P., et al. (2017). Theta-burst microstimulation in the human entorhinal area improves memory specificity. Elife *6*, e29515. https://doi.org/10.7554/elife.29515.

23. Solomon, E.A., Sperling, M.R., Sharan, A.D., Wanda, P.A., Levy, D.F., Lyalenko, A., Pedisich, I., Rizzuto, D.S., and Kahana, M.J. (2021). Theta-burst stimulation entrains frequency-specific oscillatory responses. Brain Stimul *14*, 1271–1284. https://doi.org/10.1016/j.brs.2021.08.014.

24. Herrero, J.L., Smith, A., Mishra, A., Markowitz, N., Mehta, A.D., and Bickel, S. (2021). Inducing neuroplasticity through intracranial θ-burst stimulation in the human sensorimotor cortex. J. Neurophysiol. *126*, 1723–1739. https://doi.org/10.1152/jn.00320.2021.

25. Huang, Y., Zelmann, R., Hadar, P., Dezha-Peralta, J., Richardson, R.M., Williams, Z.M., Cash, S.S., Keller, C.J., and Paulk, A.C. (2024). Theta-burst direct electrical stimulation remodels human brain networks. Nat. Commun. *15*, 6982. https://doi.org/10.1038/s41467-024-51443-1.

26. Keller, C.J., Truccolo, W., Gale, J.T., Eskandar, E., Thesen, T., Carlson, C., Devinsky, O., Kuzniecky, R., Doyle, W.K., Madsen, J.R., et al. (2010). Heterogeneous neuronal firing patterns during interictal epileptiform discharges in the human cortex. Brain *133*, 1668–1681. https://doi.org/10.1093/brain/awq112.

27. Quyen, M.L.V., Bragin, A., Staba, R., Crépon, B., Wilson, C.L., and Engel, J. (2008). Cell Type-Specific Firing during Ripple Oscillations in the Hippocampal Formation of Humans. J. Neurosci. *28*, 6104–6110. https://doi.org/10.1523/jneurosci.0437-08.2008.

28. Peyrache, A., Dehghani, N., Eskandar, E.N., Madsen, J.R., Anderson, W.S., Donoghue, J.A., Hochberg, L.R., Halgren, E., Cash, S.S., and Destexhe, A. (2012). Spatiotemporal dynamics of neocortical excitation and inhibition during human sleep. Proc. Natl. Acad. Sci. *109*, 1731–1736. https://doi.org/10.1073/pnas.1109895109.

29. Barthó, P., Hirase, H., Monconduit, L., Zugaro, M., Harris, K.D., and Buzsáki, G. (2004). Characterization of Neocortical Principal Cells and Interneurons by Network Interactions and Extracellular Features. J Neurophysiol *92*, 600–608. https://doi.org/10.1152/jn.01170.2003.

30. Keller, C.J., Huang, Y., Herrero, J.L., Fini, M., Du, V., Lado, F.A., Honey, C.J., and Mehta, A.D. (2018). Induction and quantification of excitability changes in human cortical networks. J Neurosci *38*, 1088–17. https://doi.org/10.1523/jneurosci.1088-17.2018.

31. Huang, Y., Hajnal, B., Entz, L., Fabó, D., Herrero, J.L., Mehta, A.D., and Keller, C.J. (2019). Intracortical Dynamics Underlying Repetitive Stimulation Predicts Changes in Network Connectivity. J Neurosci *39*, 6122–6135. https://doi.org/10.1523/jneurosci.0535-19.2019.

32. Hebb, D.O. (1949). The organization of behavior; A neuropsychological theory (John Wiley and Sons, Inc.) https://doi.org/10.1002/sce.37303405110.

33. Inman, C.S., Bijanki, K.R., Bass, D.I., Gross, R.E., Hamann, S., and Willie, J.T. (2020). Human amygdala stimulation effects on emotion physiology and emotional experience. Neuropsychologia *145*, 106722. https://doi.org/10.1016/j.neuropsychologia.2018.03.019.

34. Inman, C.S., Hollearn, M.K., Augustin, L., Campbell, J.M., Olson, K.L., and Wahlstrom, K.L. (2023). Discovering how the amygdala shapes human behavior: From lesion studies to neuromodulation. Neuron. https://doi.org/10.1016/j.neuron.2023.09.040.

35. Romero, M.C., Merken, L., Janssen, P., and Davare, M. (2022). Neural effects of continuous theta-burst stimulation in macaque parietal neurons. eLife *11*, e65536. https://doi.org/10.7554/elife.65536.

36. Krause, M.R., Vieira, P.G., Csorba, B.A., Pilly, P.K., and Pack, C.C. (2019). Transcranial alternating current stimulation entrains single-neuron activity in the primate brain. Proc. Natl. Acad. Sci. *116*, 5747–5755. https://doi.org/10.1073/pnas.1815958116.

37. Fehring, D.J., Yokoo, S., Abe, H., Buckley, M.J., Miyamoto, K., Jaberzadeh, S., Yamamori, T., Tanaka, K., Rosa, M.G.P., and Mansouri, F.A. (2024). Direct current stimulation modulates prefrontal cell activity and behaviour without inducing seizure-like firing. Brain, awae273. https://doi.org/10.1093/brain/awae273.

38. Youssef, D., Wittig, J.H., Jackson, S., Inati, S.K., and Zaghloul, K.A. (2023). Neuronal Spiking Responses to Direct Electrical Microstimulation in the Human Cortex. J. Neurosci. *43*, 4448–4460. https://doi.org/10.1523/jneurosci.1666-22.2023.

39. Solomon, E.A., Kragel, J.E., Gross, R., Lega, B., Sperling, M.R., Worrell, G., Sheth, S.A., Zaghloul, K.A., Jobst, B.C., Stein, J.M., et al. (2018). Medial temporal lobe functional connectivity predicts stimulation-induced theta power. Nat. Commun. *9*, 4437. https://doi.org/10.1038/s41467-018-06876-w.

40. Stiso, J., Khambhati, A.N., Menara, T., Kahn, A.E., Stein, J.M., Das, S.R., Gorniak, R., Tracy, J., Litt, B., Davis, K.A., et al. (2019). White Matter Network Architecture Guides Direct Electrical Stimulation through Optimal State Transitions. Cell Reports *28*, 2554-2566.e7. https://doi.org/10.1016/j.celrep.2019.08.008.

41. Keller, C.J., Bickel, S., Entz, L., Ulbert, I., Milham, M.P., Kelly, C., and Mehta, A.D. (2011). Intrinsic functional architecture predicts electrically evoked responses in the human brain. Proc. Natl. Acad. Sci. *108*, 10308–10313. https://doi.org/10.1073/pnas.1019750108.

42. Fox, K.C.R., Shi, L., Baek, S., Raccah, O., Foster, B.L., Saha, S., Margulies, D.S., Kucyi, A., and Parvizi, J. (2020). Intrinsic network architecture predicts the effects elicited by intracranial electrical stimulation of the human brain. Nat. Hum. Behav. *4*, 1039–1052. https://doi.org/10.1038/s41562-020-0910-1.

43. Lee, S.Y., Kozalakis, K., Baftizadeh, F., Campagnola, L., Jarsky, T., Koch, C., and Anastassiou, C.A. (2024). Cell-class-specific electric field entrainment of neural activity. Neuron. https://doi.org/10.1016/j.neuron.2024.05.009.

44. Zheng, J., Stevenson, R.F., Mander, B.A., Mnatsakanyan, L., Hsu, F.P.K., Vadera, S., Knight, R.T., Yassa, M.A., and Lin, J.J. (2019). Multiplexing of Theta and Alpha Rhythms in the Amygdala-Hippocampal Circuit Supports Pattern Separation of Emotional Information. Neuron *102*, 887-898.e5. https://doi.org/10.1016/j.neuron.2019.03.025.

45. Shoham, S., O'Connor, D.H., and Segev, R. (2006). How silent is the brain: is there a "dark matter" problem in neuroscience? J. Comp. Physiol. A *192*, 777–784. https://doi.org/10.1007/s00359-006-0117-6.

46. Bass, D.I., Partain, K.N., and Manns, J.R. (2012). Event-Specific Enhancement of Memory via Brief Electrical Stimulation to the Basolateral Complex of the Amygdala in Rats. Behav. Neurosci. *126*, 204–208. https://doi.org/10.1037/a0026462.

47. Bass, D.I., Nizam, Z.G., Partain, K.N., Wang, A., and Manns, J.R. (2014). Amygdala-mediated enhancement of memory for specific events depends on the hippocampus. Neurobiol. Learn. Mem. *107*, 37–41. https://doi.org/10.1016/j.nlm.2013.10.020.

48. Bass, D.I., and Manns, J.R. (2015). Memory-Enhancing Amygdala Stimulation Elicits Gamma Synchrony in the Hippocampus. Behav. Neurosci. *129*, 244–256. https://doi.org/10.1037/bne0000052.

49. Manns, J.R., and Bass, D.I. (2016). The Amygdala and Prioritization of Declarative Memories. Curr. Dir. Psychol. Sci. *25*, 261–265. https://doi.org/10.1177/0963721416654456.

50. Kajikawa, Y., and Schroeder, C.E. (2011). How Local Is the Local Field Potential? Neuron *72*, 847–858. https://doi.org/10.1016/j.neuron.2011.09.029.

51. Manning, J.R., Jacobs, J., Fried, I., and Kahana, M.J. (2009). Broadband Shifts in Local Field Potential Power Spectra Are Correlated with Single-Neuron Spiking in Humans. J. Neurosci. *29*, 13613–13620. https://doi.org/10.1523/jneurosci.2041-09.2009.

52. Herreras, O. (2016). Local Field Potentials: Myths and Misunderstandings. Front. Neural Circuits *10*, 101. https://doi.org/10.3389/fncir.2016.00101.

53. Teleńczuk, M., Teleńczuk, B., and Destexhe, A. (2020). Modelling unitary fields and the single-neuron contribution to local field potentials in the hippocampus. J. Physiol. *598*, 3957–3972. https://doi.org/10.1113/jp279452.

54. Geva-Sagiv, M., Mankin, E.A., Eliashiv, D., Epstein, S., Cherry, N., Kalender, G., Tchemodanov, N., Nir, Y., and Fried, I. (2023). Augmenting hippocampal–prefrontal neuronal synchrony during sleep enhances memory consolidation in humans. Nat Neurosci, 1–11. https://doi.org/10.1038/s41593-023-01324-5.

55. Jacobs, J., Kahana, M.J., Ekstrom, A.D., and Fried, I. (2007). Brain Oscillations Control Timing of Single-Neuron Activity in Humans. J. Neurosci. *27*, 3839–3844. https://doi.org/10.1523/jneurosci.4636-06.2007.

56. Rutishauser, U., Ross, I.B., Mamelak, A.N., and Schuman, E.M. (2010). Human memory strength is predicted by theta-frequency phase-locking of single neurons. Nature *464*, 903–907. https://doi.org/10.1038/nature08860.

57. Yoo, H.B., Umbach, G., and Lega, B. (2021). Neurons in the human medial temporal lobe track multiple temporal contexts during episodic memory processing. NeuroImage *245*, 118689. https://doi.org/10.1016/j.neuroimage.2021.118689.

58. Schonhaut, D.R., Rao, A.M., Ramayya, A.G., Solomon, E.A., Herweg, N.A., Fried, I., and Kahana, M.J. (2024). MTL neurons phase-lock to human hippocampal theta. eLife *13*, e85753. https://doi.org/10.7554/elife.85753.

59. Hasselmo, M.E., Bodeln, C., and Wyble, B.P. (2002). A Proposed Function for Hippocampal Theta Rhythm: Separate Phases of Encoding and Retrieval Enhance Reversal of Prior Learning. Neural Comput. *14*, 793–817. https://doi.org/10.1162/089976602317318965.

60. Hasselmo, M.E. (2005). What is the function of hippocampal theta rhythm?—Linking behavioral data to phasic properties of field potential and unit recording data. Hippocampus *15*, 936–949. https://doi.org/10.1002/hipo.20116.

61. Hasselmo, M.E., and Stern, C.E. (2014). Theta rhythm and the encoding and retrieval of space and time. Neuroimage *85*, 656–666. https://doi.org/10.1016/j.neuroimage.2013.06.022.

62. Siegle, J.H., and Wilson, M.A. (2014). Enhancement of encoding and retrieval functions through theta phase-specific manipulation of hippocampus. Elife *3*, e03061. https://doi.org/10.7554/elife.03061.

63. Virtanen, P., Gommers, R., Oliphant, T.E., Haberland, M., Reddy, T., Cournapeau, D., Burovski, E., Peterson, P., Weckesser, W., Bright, J., et al. (2020). SciPy 1.0: fundamental algorithms for scientific computing in Python. Nat Methods *17*, 261–272. https://doi.org/10.1038/s41592-019-0686-2.

64. Seabold, S., and Perktold, J. (2010). Statsmodels: Econometric and Statistical Modeling with Python. Proc 9th Python Sci Conf, 92–96. https://doi.org/10.25080/majora-92bf1922-011.

65. Waskom, M. (2021). seaborn: statistical data visualization. J. Open Source Softw. *6*, 3021. https://doi.org/10.21105/joss.03021.

66. Davis, T.S., Caston, R.M., Philip, B., Charlebois, C.M., Anderson, D.N., Weaver, K.E., Smith, E.H., and Rolston, J.D. (2021). LeGUI: A Fast and Accurate Graphical User Interface for Automated Detection and Anatomical Localization of Intracranial Electrodes. Front. Neurosci. *15*, 769872. https://doi.org/10.3389/fnins.2021.769872.

67. Mercier, M.R., Dubarry, A.-S., Tadel, F., Avanzini, P., Axmacher, N., Cellier, D., Vecchio, M.D., Hamilton, L.S., Hermes, D., Kahana, M.J., et al. (2022). Advances in human intracranial electroencephalography research, guidelines and good

practices. Neuroimage *260*, 119438. https://doi.org/10.1016/j.neuroimage.2022.119438.

68. Suppa, A., Huang, Y.-Z., Funke, K., Ridding, M.C., Cheeran, B., Lazzaro, V.D., Ziemann, U., and Rothwell, J.C. (2016). Ten Years of Theta Burst Stimulation in Humans: Established Knowledge, Unknowns and Prospects. Brain Stimul. *9*, 323–335. https://doi.org/10.1016/j.brs.2016.01.006.

69. Hanslmayr, S., Staresina, B.P., and Bowman, H. (2016). Oscillations and Episodic Memory: Addressing the Synchronization/Desynchronization Conundrum. Trends Neurosci *39*, 16–25. https://doi.org/10.1016/j.tins.2015.11.004.

70. Shoham, S., Fellows, M.R., and Normann, R.A. (2003). Robust, automatic spike sorting using mixtures of multivariate t-distributions. J. Neurosci. Methods *127*, 111–122. https://doi.org/10.1016/s0165-0270(03)00120-1.